the slotted diaphragm depends on the factors such as the thickness of the plate, width & depth of the slots, position of the slots and degree of freedom of the membrane. These slots can be machined using tool-based micromachining setup. The material used for the slotted diaphragm is Acrylic since it has good flexural strength, high impact resistance, transparent and lightweight in nature. Also, acrylic is chemically stable with most of the chemicals and can be machined easily. The material properties of acrylic are given in Table 2.

Table 2: Properties of slotted diaphragm and Check Valve

	Properties	
	Slotted Diaphragm	**Check Valve (cellulose acetate)**
Young's modulus (GPa)	3	2.4
Density (kg/m3)	1200	1280
Poisson's ratio	0.35	0.38

The thickness of the acrylic diaphragm plate is 5mm on which slots are machined in such a way so as to obtain the effective thickness of 0.8 mm. Outer diameter is 50mm and effective centre diameter is 38mm. The diaphragm is fixed to the pump chamber by means of M3 screws and the rubber seal is used for proper sealing. When a voltage is applied to electromagnet it produces a magnetic field which attracts the small metal plate screwed to the upper face of diaphragm thereby causing the deflection of the diaphragm. The maximum displacement is obtained at the centre region of the diaphragm. Analysis has been carried out in ANSYS analysis software to select the slot dimensions in order to get a required deflection. Figures 4(a) and (b) shows the 3D model and fabricated slotted diaphragm.

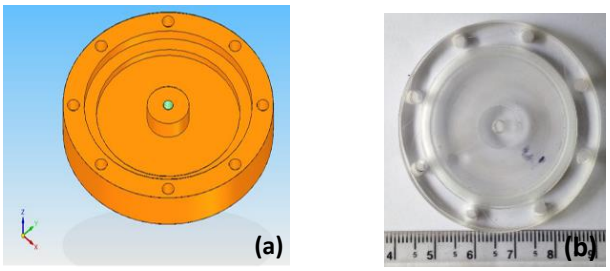

Figure 4: (a) Isometric view of diaphragm, (b) Fabricated Diaphragm

Stiffness is an important factor while designing the diaphragm if the stiffness is high the displacement of the diaphragm will be very less. So stiffness value must be as small as possible for the applied load. Load vs displacement analysis is done to find the stiffness of the diaphragm. Finite element analysis for different slot width, slot depth and thickness of the diaphragm is done using ANSYS simulation software. Acrylic is the material used and their material properties are shown in Table 2.

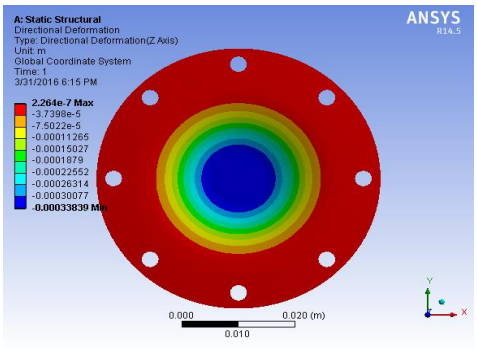

Figure 5: Ansys analysis of diaphragm

Figure 5 shows the analysis of diaphragm. An analysis is conducted by fixing the diaphragm at the holes and applying the load at the centre region. We obtained 338.39µm deflection for the applied 20N load which yields to the stiffness value of 0.059N/µm which is more than the normal circular plates fixed at edges. From the analysis, it is found that the deflected diaphragm takes the shape of the cone as shown in Figure 6. Therefore, the volume displaced due to the deflection of the diaphragm can be calculated by considering the volume of the frustum of a cone using Eq (1).

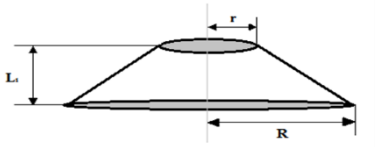

Figure 6: Shape of the diaphragm after deflection

Therefore the volume of fluid displaced per stroke is given by,

$$v = \pi^3 \times L_1 \times \left(R_2 + r_2 + R \times r\right) \quad \ldots\ldots (1)$$

Where L_1 stands for Deflection of the diaphragm, R is the effective radius of the diaphragm and r is a radius at the top of a frustum of the cone in the deflected position

4. DESIGN OF CHECK VALVE

The passive valves are integrated with micropump for the necessity of flow rectification during the working. These valves are independent of the physical actuator for its operation. The main requirement of the passive valve along with flow rectification is to reduce the leakage during backflow or to avoid backflow. These valves will be actuated by the forces that are produced during the pumping in the pumping cycle which either stops or allows the fluid supply. Valve opening should be carried with less pressure. The passive valve ideally should have low spring constant and low young modulus leading to better functionality. The different types of passive valves include V shape, membrane type, disc, cantilever, ring etc. In present work, check valve designed using cellulose acetate film. The dimensions of the check valve are 8*8mm. The proposed check valve design and fabricated check valve are shown in Figures 7 (a) and (b) respectively

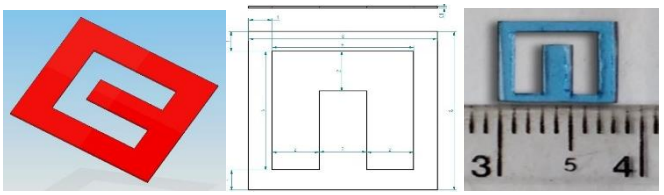

(a) Isometric view **(b)** 2D view **(c)** Fabricated

Figure 7: Check valve

Load vs deflection analysis is done to find the stiffness of the check valve. Finite element analysis for different thickness of check valve is done using ANSYS simulation software. Cellulose acetate (OHP sheet) is the material used and their material properties are shown in Table 2. During the analysis, one end of the check valve is fixed and deflected portion is subjected to load shown in Figure.8.

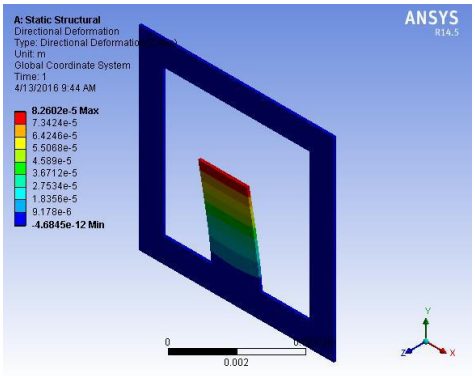

Figure 8: Ansys analysis of check valve

5. TOOL BASED MICROMACHINING SETUP FOR FABRICATING ELECTROMAGNETIC PUMP

Figure 9 shows a block diagram of a prototype mechanical micromachining centre with the piezo-actuated workpiece feeding system. It consists of an interchangeable spindle to rotate the micro-milling/drilling tool at 24,000 rpm, 60,000rpm, and 1,00,000 rpm. The spindle speed is controlled by a variable frequency drive (CGK2D00150, 1.5kW, 0-240V, 0-1500Hz, 7.0A). An analogue output signal proportional to the rotational speed of high-speed spindle generated by variable frequency drive is acquired through a data acquisition system (NI-USB 6251, 1.25Ms/sec sampling rate, 16 Analog inputs, 2 Analog outputs, 16 Bit resolution, Voltage range-10V to +10V). This analogue data is further converted in to spindle speed through calibration. A contact detection system is developed to detect the contact between the tool and the workpiece. Peltier based liquid cooling system is developed to control the spindle temperature at a set value. Compressed air cooled to a temperature of sub-zero degree centigrade is used as a coolant to reduce the temperature at the tool-workpiece interface during micromachining operation. An APA230L piezoactuator (Displacement 236µm, -20 to 150V, 2-4nm resolution, from Cedrat Technologies, France) is used to feed the workpiece in Z-direction towards the tool. The Z- direction displacement of the workpiece is measured by using Laser displacement sensor (ILD 2220-20, Measuring Range 20mm, 0.3µm Resolution, from Micro-Epsilon, Germany).

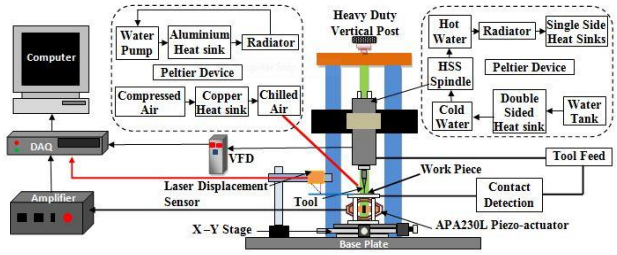

Figure 9: Tool based mechanical micromachining setup [21]

6. RESULTS AND DISCUSSION

Figure 10 shows the displacement of the diaphragm for the applied load. The load is plotted along x-axis and displacement is plotted along the y-axis. From this graph, the stiffness of diaphragm obtained is 0.059 N/µm. As the load increases the displacement of diaphragm increases linearly.

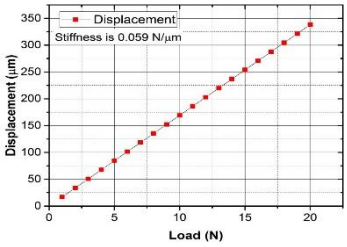

Figure 10: Load vs Displacement

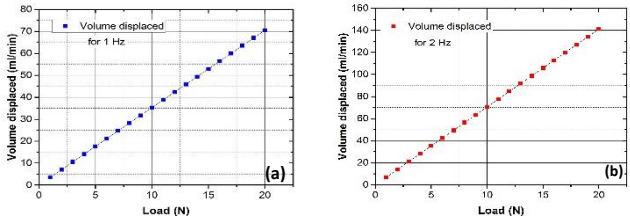

Figure 11: (a) Load vs volume displaced plot for 1Hz, (b) Load vs Volume displaced plot for 2 Hz

The graph is drawn by taking a load in x-axis and volume displaced in the y-axis. From observations, it can be seen that by an increase in load the volume displaced is also increases linearly. From theoretical volume displacement calculations extreme flow rate of 70.546 ml/min is found for the applied load of 20N when 1 Hz frequency is applied and 141.092 ml/min when 2 Hz frequency is applied shown in Figure 11.

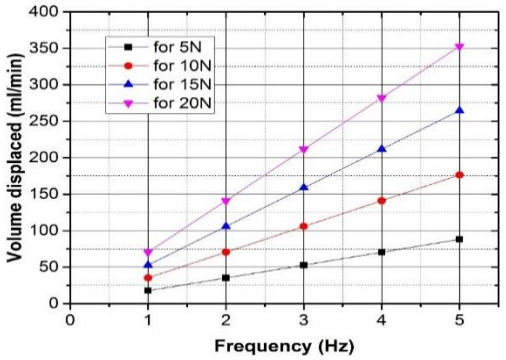

Figure 12: Frequency vs Volume displacement plot or1Hz

From Figure 12 it is evident that as the frequency of actuation increases volume displaced will also increase but higher frequency cannot be achievable due to the hysteresis limitation of the electromagnet used in micropump. Hence optimum frequency range is maintained in order to get the desired output. During the analysis of check valve, we obtained 82.602µm deflection for an applied 0.01N load which yields to the stiffness value of 0.00012N/µm shown in Figure. 13.

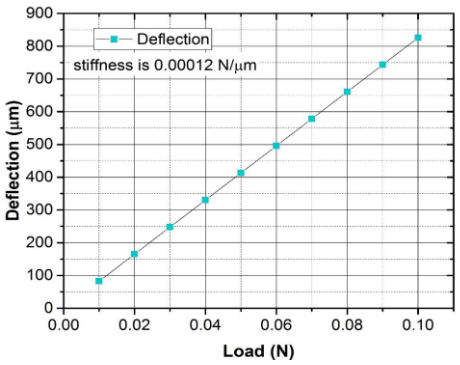

Figure 13: Load vs deflection plot for check valve

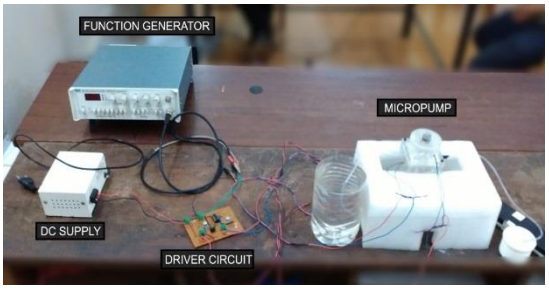

Figure 14: Experimental setup

Figure 14 shows the experimental setup for the testing of the electromagnetic pump. The electromagnetic pump was supplied with an input voltage of 6V-12V and at different frequencies starting from 1Hz to 5Hz with the increment of 1Hz and the head developed was noted. Figure 15 shows the head developed in millimetres with different frequencies.

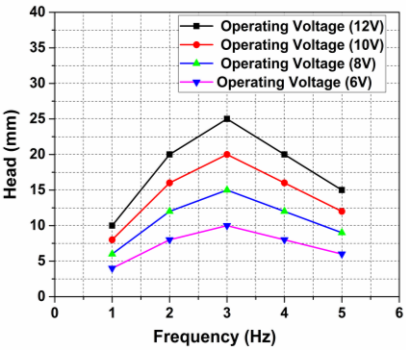

Figure 15: Plot of head vs frequency included in the electromagnetic pump

From the above plot, it is evident that the maximum head developed is at a frequency of 3Hz which the optimum frequency for this configuration of the electromagnetic pump is. The maximum head obtained at this optimal frequency is 25mm. Finally, in order to measure the flow rate of the electromagnetic pump the pump was actuated at 3Hz frequency alone by varying the head of the micropump from 4 to 20mm.

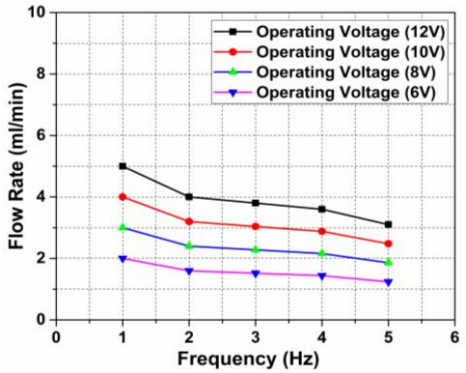

Figure 16: Plot of flow rate vs head actuated at 3Hz frequency

Figure 16 plot shows a decreasing trend throughout, as the head is increased the flow rate has decreased. Ideally the flow obtained should have been to till head of 25mm (Fig.15) but from Fig.16 the flow rate is calculated till 20mm this is due to time required in order to get the flow is more as the head is increased, and for the fact that flow measuring technique should be advanced for the measuring of the flow rates at high heads because the flow obtained will be millilitres.

7. CONCLUSIONS

A novel electromagnetically actuated micropump is designed and fabricated using tool based micromachining setup. Finite element analysis of the check valve and the diaphragm is carried out using ANSYS software to find the stiffness of the check valve and diaphragm. Experiments on electromagnetic micropump were carried out at a voltage of 6V-12V and frequency was varied from 1-5Hz to find the optimum frequency. The optimum frequency for the pump operation was found to be 3Hz generating a maximum head of 25mm. The flow rates were obtained at an optimized frequency of 3Hz by varying the head and were observed that the flow rate was decreasing with an increase in head.

REFERENCES

[1] Woias, P. 2005. Micropumps-past, progress and future prospects. Sensors and Actuators B., 105 (1), pp. 28-38.

[2] Zhou, Y., Amirouche, F. 2011. An Electromagnetically-Actuated All-PDMS Valve less Micropump for Drug Delivery. Micromachines, 2 (3), pp. 345-355.

[3] Pan, T., McDonald, S.J., Kai, E.M., Ziaie, B. 2005. A magnetically driven PDMS micropump with ball check-valves. Journal of Micromechanics and Microengineering, 15 (5), pp. 1021-1026.

[4] Khoo, M., LIuA, C. 2000. Novel micromachined magnetic membrane microfluid pump", Proceedings of the 22nd Annual EMBS International Conference. Chicago IL, pp. 2394-2397.

[5] Yamahata, C., Lotto, C., Al-Assaf, E., Gijs, M.A.M. 2004. A PMMA valve less micropump using electromagnetic actuation. Microfluidics and Nanofluidics, 1 (3), pp. 197–207.

[6] Shen, C.Y., Hsien-kuang, L. 2010. Innovative Composite PDMS Micropump with Electromagnetic Drive. Sensors and Materials, 22 (2), pp. 85–100.

[7] Tetteh, E.A., Boatemaa, M.A., Martinson, E.O. 2014. A Review of Various Actuation Methods in Micropumps for Drug Delivery Applications. 11th International Conference on Electronics, Computer and Computation, 1-4.

[8] Guo, S., Pei, Z., Wang, T., Ye, X. 2007. Development of Pulseless Output Micropump Using Magnet Solenoid Actuator. International Conference on Mechatronics and Automation., Harbin, China, pp. 1079-1084.

[9] Guo, S., Wang, J., Pan, Q., Guo, J. 2006. Solenoid Actuator-based Novel Type of Micropump. IEEE International Conference on Robotics and Biomimetics., Kunming, China, pp. 1281-1286.

[10] Guu, Y.H., Hocheng, H., Chang, C.H. 2008. Study of Piezoelectrically Actuated Micropumps with Multiple Parallel Chambers. Materials and Manufacturing Processes, 23 (2), pp. 209–214.

[11] Liu, G., Yang, Z., Liu, J., Li, X., Wang, H., Zhao, T., Yang, X. 2014. A low cost, high performance insulin delivery system based on PZT actuation. Microsystem Technology, 20 (12), pp. 2287–2294.

[12] Nguyen, N.T., Huang, X., Chuan, T.K. 2002. MEMS-Micropumps: A Review. Journal of fluids engineering, 124 (2), pp. 384-392.

[13] Amirouche, F., Zhou, Y., Johnson, T. 2009. Current micropump technologies and their biomedical applications. Microsystems Technologies, 15 (5), pp. 647–666.

[14] Cao, L., Mantell, S., Polla, D. 2001. Design and simulation of an implantable medical drug delivery system using micro electromechanical systems technology. Sensors and Actuators, 94 (1-2), pp. 117-125.

[15] Samad, M.F., Kouzani, A.Z. 2013. Integrated microfluidic drug delivery devices; a component view. Microsystem technology, 19 (7), pp. 957-970.

[16] Jivani, R.R., Lakhtaria, G.J., Patadiya, D.D., Patel, L.D., Jivani, N.P., Jhala, B.P. 2016. Biomedical Microelectromechanical Systems (BioMEMS): Revolution in Drug Delivery and Analytical Techniques. Saudi Pharmaceutical Journal, 24 (1), pp. 1-20.

[17] Shuxiang, G., Junsei, O., Fukuda, T. 2003. A novel type of micropump using SMA actuator for microflow application. Proceedings of 2003 International Symposium on Micromechatronics, pp. 45-50.

[18] Yamhanta, C., Lacharme, F., Gijs, M.A.M. 2005. Glass valvelessmicropump using electromagnetic actuation. Microelectronic Engineering, 78-79, pp. 132-137.

[19] Diaz, J., Lopera, J.M., Pernia, A.M., Nuno, F., Martinez, J.A., Comas, J.V., Gallatti, L. 2007. A micropump for pulmonary blood flow regulation. IEEE Industrial Electronics Magazine, 1 (1), pp. 39-44.

[20] Shoji, S., Eshashi, M. 1994. Microflow devices and systems. Journal of micromechanics and microengineering, 4 (4), pp. 157-171.

Veeresha, R.K., Muralidhara, Rao, R. 2014. Development of Tool Based Micromilling/ Microdrilling Machine with Piezoactuated Workpiece Feeding System. Applied Mechanics and Materials, 592-594, pp. 164-169.